IEEE Robotics & Automation Magazine (RAM) paper, presented at ICRA 2024, Yokohama, Japan. Cite as RAM paper.

Terrain-adaptive Locomotion Control for an Underwater Hexapod Robot: Sensing Leg-terrain Interaction with Proprioceptive Sensors

Lepeng Chen, Rongxin Cui, Weisheng Yan, Hui Xu, Shouxu Zhang, Haitao Yu

***Abstract*—Underwater hexapod robot, driven by six C-shaped legs and eight thrusters, has the potential to traverse diverse terrains with unknown deformable properties, which can lead to unknown leg-terrain interaction forces. However, it is hard to use exteroceptive sensors such as cameras and sonars to recognize these properties. Here, we propose a method to perceive the interaction forces and feed them into a controller for determining thrust inputs. The key idea lies in using supervised learning to obtain the properties from reliable proprioceptive sensory data. First, we propose a new expression called Zero Moment Point (ZMP) bias that can indirectly represent the leg-terrain interaction force, removing the effects caused by gravity, buoyancy, and thrust. Second, we gather a walking cycle's discrete ZMP biases and then parameterize them as polynomials. Third, we use several previous walking cycles' parameterized biases to predict the current walking cycle's biases to generate the needed pitch and roll moments. Finally, we propose a terrain-adaptive locomotion controller for the robot, which incorporates these moments into a base control module and uses thrust to compensate for the interaction force for smooth walking. Extensive indoor pool and wild lake hardware experiments confirm our method's effectiveness.**

***Index Terms*—Underwater hexapod robot, ZMP bias, C-shaped leg, leg-terrain interaction force.**

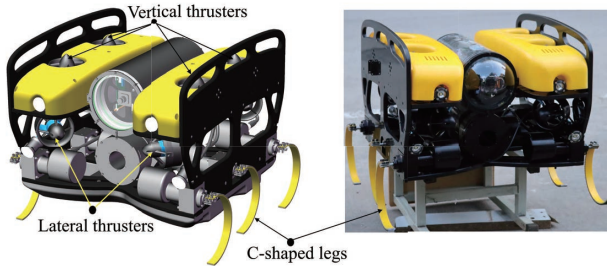

Fig. 1. Underwater hexapod robot with six C-shaped legs and eight thrusters.

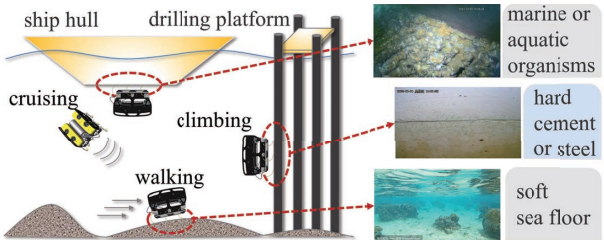

Fig. 2. Illustration of three terrains with different deformable properties.

I. INTRODUCTION

Interest in underwater robots is growing at a rapid pace due to the need to explore and operate in the underwater environment. According to whether shore-based systems operate the robots, they can be divided into two categories, i.e., remotely operated vehicles (ROVs) and autonomous underwater vehicles (AUVs). Some tasks, such as hull cleaning, fracture detection, and damage restoration, require the robot to adhere tightly to the underwater structure's surface to perform meticulous small-range operations, whereas ROVs or AUVs cannot get attached to these surfaces. Thus, as shown in Fig. 1, we develop an underwater robot with eight thrusters and six C-shaped legs. Fig. 2 shows the diagram that the robot walks on the surfaces of a hull, a drilling platform, and a sea floor, assisted by eight thrusters. The hull surface may be covered with marine or aquatic organisms, and their deformation mechanisms are difficult to model. The soft sea floor consists of multiple substances, such as soil, sand, and decomposing organics, and their deformable properties are unknown. In addition, the drilling platform's surface is also with unknown deformable properties. Impacting with or rolling on these surfaces leads to uncertain leg-terrain interaction forces, also called interaction dynamics. Due to the uncertain interaction dynamics, unexpected sharp shaking or even loss of balance may happen when the robot walks on these underwater structures.

Two kinds of approaches can cope with the uncertain interaction forces, i.e., passive and active ones. The passive approach smoothes walking by designing the foot's type [1] and geometry [2] according to apriori geological features. The active approach aims to design the control methods for legged robots and use joint torques to compensate for uncertain interaction forces, including model-based control [3]–[6], energy-based control [7]–[10] and learning-based control [11]–[13].

Using the modeled interaction dynamics between planar leg and granular terrain, Xiong *et al.* [3] analyze a bipedal robot's stability margin by calculating the admissible ZMP region and present an optimal controller to generate the stable gaits for walking. Boswort *et al.* [4] present a novel locomotion controller to traverse unknown terrains smoothly for Cheetah robot by assessing the stability in response to self-disturbances

*This work was supported in part by the National Natural Science Foundation of China (NSFC) under grant 61733014, grant U1813225, grant U22A2066 and grant 62103182, and in part by the Doctorate Foundation of Northwestern Polytechnical University under grant CX201904.
(Corresponding author: Rongxin Cui.)
All authors are with School of Marine Science and Technology, Northwestern Polytechnical University, Xi'an 710072, China. e-mail: r.cui@nwpu.edu.cn.

IEEE Robotics & Automation Magazine (RAM) paper, presented at ICRA 2024, Yokohama, Japan. Cite as RAM paper.

and peak accelerations. Two promising whole-body optimal locomotion controllers [5], [6] are presented by incorporating the modeled spring-damper-based interaction dynamics and estimating stiffness and damping parameters online.

Based on the multipart pronking controller in [7], a promising controller is presented for a monopod robot by compensating for the energy dissipation of the terrain's permanent deformation online [8]. It is extended in [9] to enable the quadruped robot with a reaction wheel to walk on viscoplastic terrain with the desired forward velocity. Vasilopoulos *et al.* [10] use force sensors installed on the leg's bottom to measure leg-terrain interaction forces for energy dissipation calculating.

The learning methods use collected sensory data to learn the control policy of smoothly traversing unknown terrain. In [11], a planetary rover uses a multi-task Gaussian Process (GP) based regression method to map the correlation between terrain deformation and exteroceptive, proprioceptive sensory data to estimate its traversability. Chang *et al.* [12] use the GP-based regression method to learn the unknown interaction forces between 1-D jumper and deformable terrain iteratively and then design an optimal controller for jumping with a desired height. Lee *et al.* [13] propose a novel robust reinforcement learning control method to find the map between control inputs and proprioceptive sensory data for natural terrain traversing.

The methods in [3]–[9] need partial or even complete knowledge of the leg-terrain interaction dynamics. In fact, it is hard to obtain prior knowledge due to the underwater environment. Several promising methods use exteroceptive sensory data to perceive and recognize terrain properties indirectly for ground robots, and the used sensors consist of three categories, e.g., cameras [11], [12], [14], force sensors [3], [10], [15]–[17] and microphones [18]. Although vision-based methods can recognize terrain's deformable properties by capturing its texture information, they are hard to use underwater because attenuation and multiple scattering dramatically disrupt the visual data. Also, acoustics-based methods use a microphone to recognize acoustic features during touching to perceive the terrain properties. Although the sonar can perceive the terrain's geometric information underwater, it fails to extract the deformable properties. Finally, unlike common flat or spherical legs, a C-shaped leg rolls on the underwater terrain for walking, and a flexible striped force sensor needs to be mounted on its touching side. However, no sufficiently precise and ready-made force sensor can be directly used for an underwater C-shaped leg.

In this paper, we present a terrain-adaptive locomotion controller for the robot. Fig. 3 and Table I present its diagram and the comparison of related works and our work. The contributions are listed as follows.

1) We present a new ZMP bias expression that can perceive the leg-terrain interaction force using proprioceptive sensory data.
2) We present an adaptive controller that uses leg torques to achieve basic legged locomotion and employs thruster forces to compensate for the interaction force.
3) We perform extensive hardware experiments on an indoor pool and lake to demonstrate our method's effectiveness.

TABLE I
COMPARISON OF OF RELATED CONTROL METHODS AND OUR METHOD.

	Control methods	Reliant knowledge and sensor	Contact shape
[3]	Model-based	Robot dynamics and force sensor	Flat
[4]–[6]	Model-based	Robot dynamics and interaction dynamics	Cylindrical Spherical
[7]–[9]	Energy-based	Robot dynamics and interaction dynamics	Spherical
[10]	Energy-based	Robot dynamics and force sensor	Spherical
[11], [12] [14]	Learning-based	Camera	Flat Wheeled
[15]–[17]	Learning-based	Force sensor	C-shaped Spherical
[18]	Learning-based	Microphone	Wheeled
[13]	Learning-based	Proprioceptive sensors and force sensor	Spherical
Ours	Learning-based	Robot dynamics and proprioceptive sensors	C-shaped

II. SYSTEM DESCRIPTION AND PROBLEM FORMULATION

A. System Description

As shown in Fig. 1, both thrusters and hip joints are embedded in the robot body, and each C-shaped leg is connected at the corresponding hip joint.

The equipped proprioceptive sensors include an Inertial Measurement Unit (IMU), an accelerometer, six encoders, a Doppler Velocity Log (DVL), and a depth sensor. The IMU measures the robot's orientation and angular velocity, the accelerometer measures the robot's acceleration, and the encoder measures the leg's rotation angle and velocity. The DVL is installed on the robot's bottom to measure velocity.

Fig. 4(a) shows body-fixed frame $Oxyz$, earth-fixed frame $O_0x_0y_0z_0$, and the placement of thrusters and hip joints, where the point O is located at the robot body's centroid, $l_i(i = 1, 2, \cdots, 4)$ is the distance between two adjacent thrusters, $T_i(i = 1, 2, \cdots, 8)$ denotes the force of ith thruster. $T_1, \cdots, T_4$ and $T_5, \cdots, T_8$ represent the thrusts of vertical and lateral thrusters. The six legs consist of two groups, i.e., support and swing legs, and jth leg's torque is defined as

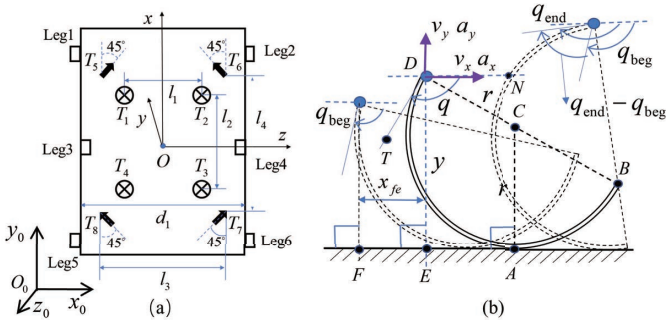

Fig. 4. Parameter definition. (a) The placement of thrusters and hip joints. (b) Robot states and leg geometric parameters.

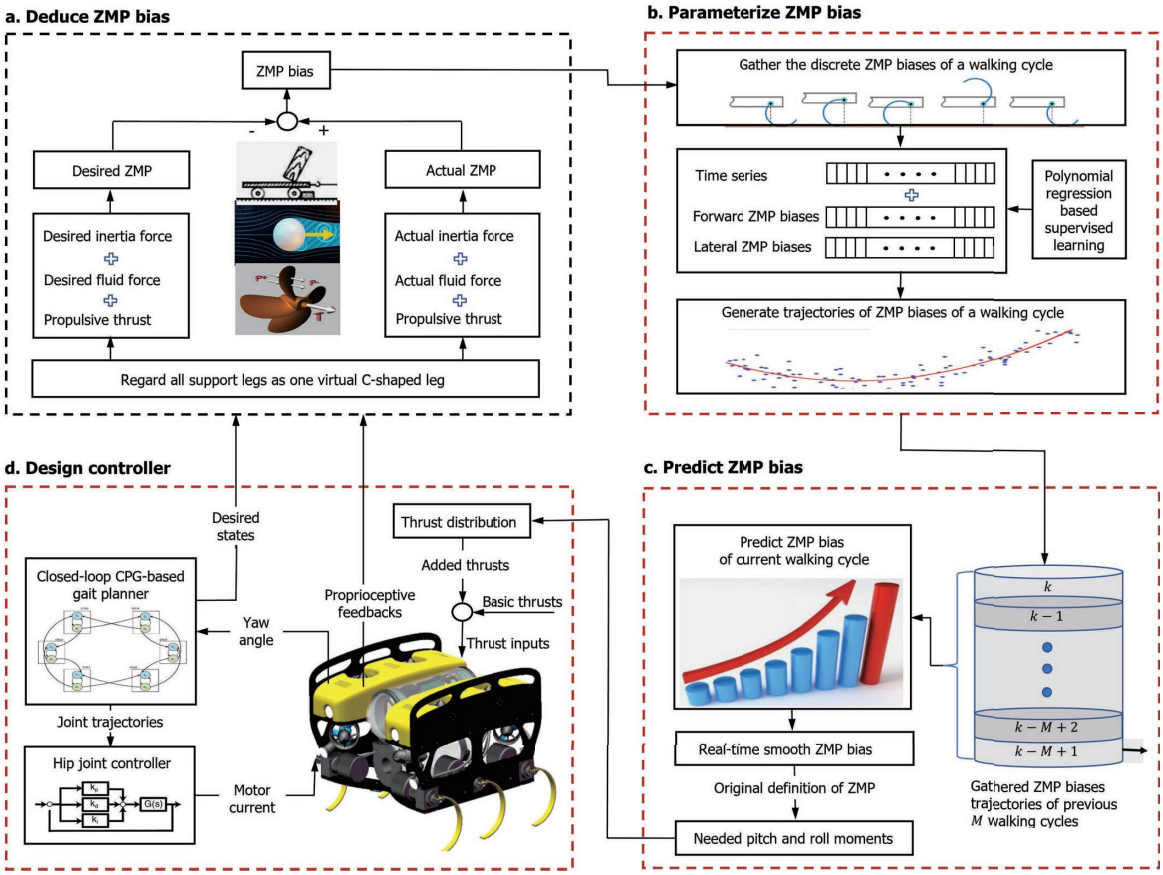

Fig. 3. Overview of our locomotion method. (a) We present the deducing process of desired ZMP, actual ZMP and ZMP bias. (b) We parameterize past walking cycles' biases by collecting locomotion data. (c) We use several parameterized results to predict the current walking cycle's ZMP bias and then calculate the needed pitch and roll moments. (d) We integrate these moments into a base control module to compensate for leg-terrain interaction dynamics.

$\tau_i (i = 1, 2, \cdots, 6)$. Then, we regard all support legs as one virtual C-shaped leg and simplify the robot as an inverted rolling pendulum, as shown in Fig. 4 (b).

Position D denotes the robot's centroid, and the robot mass is concentrated at this point. Position F is a projection of position D when the robot begins a new walking cycle. v_x and v_y are velocities along the directions of Ox and Oy, a_x and a_y represent the corresponding accelerations, y represents the height of position D, x_{fe} is the displacement of position E that relative to position F, r and $q = \angle NDT$ denote the radius and the rotation angle of the virtual leg. The two line segments DB and DT are perpendicular, that is, $\angle BDT = \frac{\pi}{2}$. $q_{\text{end}} - q_{\text{beg}}$ denotes the support angle, equals to the rotated angle of the leg during the stance phase, where q_{end} and q_{beg} denote the leg's rotation angle during the beginning and the end of one walking cycle, respectively. Similarly, the swing angle denotes the rotated angle of the leg during the swing phase. The sum of the support and swing angles is 2π.

We define the directions along axes Ox, Oy, and Oz as forward, vertical and lateral directions. In addition, the forces along axes Ox, Oy, and Oz are called forward, vertical, and lateral forces. Finally, the ZMPs along axes Ox and Oz are also defined as forward ZMP and lateral ZMP.

B. Assumptions

Assumption 1. *Six legs' inertial and fluid forces are ignored, and the robot's centroid locates at six hip joints' central point.*

Assumption 2. *The position of the buoyant center coincides with the robot's centroid.*

Assumption 3. *The deformable properties of adjacent terrains are similar, which will not change massively.*

The first assumption is logical because legs are fairly light while comparing with the robot body. Furthermore, to make our robot owns three different motion modes, the buoyant center is set close to the centroid when designing the overall mechanical structure. Finally, the First Law of Geography reveals that near two adjacent terrains are more similar than distant ones.

C. Problem Formulation

To make the robot traversing diverse terrains with unknown deformable properties smoothly, we need to address two issues. The first issue is how to use prescribed motion states, robot's velocities $v_x v_y$, v_z, accelerations a_x, a_y, a_z, and rotation angle q to perceive the leg-terrain interaction dynamics. In addition, how to design thrust T_i and torque τ_i to compensate for the perceived dynamics and follow a prescribed motion.

III. Interaction Dynamics Perception

A. Actual ZMP

ZMP is the point on the horizontal plane of $x_0O_0z_0$ where the net moment of the active forces, such as inertial force and gravity force, has no component along the axes of O_0x_0 and O_0z_0 [19]. If it belongs to the support domain, the robot is stable. Then, the relation between ZMP and the domain is often regarded as a constraint to seeking suitable control inputs or gaits for stable legged locomotion. Unlike conventional usages, this paper uses the ZMP to indirectly describe the complex reaction forces because the active forces balance the reaction forces that the terrain acts on the robot.

The ground-legged robot has two kinds of active forces, i.e., inertial force and gravity force. Apart from the two forces, our robot still has three special active forces caused by thrusters and underwater fluid environments. Specifically, Fig. 5 presents five kinds of forces that act on the hip joint of the virtual C-shaped leg, i.e., fluid forces, thrusts, inertial forces, gravity, and buoyancy, in which F_{Fx}, F_{Fy} and F_{Fz} denote forward, vertical and lateral fluid forces. F_{Tx}, F_{Ty} and F_{Tz} are forward, vertical and lateral thrusts. In addition, F_{Ix}, F_{Iy} and F_{Iz} represent forward, vertical, and lateral inertial forces. Finally, M_{Tx} and M_{Tz} denote the roll and pitch moments caused by thrusts. $G = mg$ and B are gravity and buoyancy of the robot, m is mass of the robot. Using the ZMP's original definition in [19], we can deduce

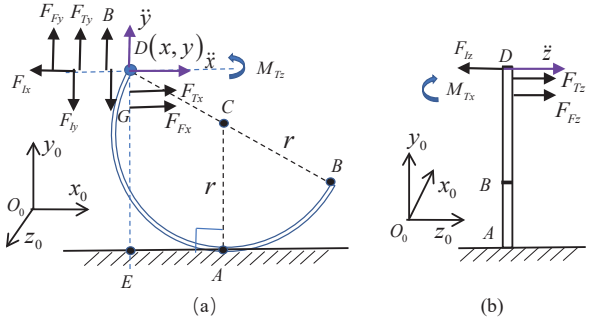

Fig. 5. Propulsive thrusts and inertial forces on the underwater hexapod robot. (a) Forces in the longitudinal plane. (b) Forces in the lateral plane.

the robot's forward and lateral ZMPs as

$$\begin{cases} X_{zmp} = x_{fe} + \dfrac{M_{Tz} - (F_{Fx} + F_{Tx} - ma_x)y}{F_{Fy} + F_{Ty} + B - m(a_y + g)} \\ Z_{zmp} = -\dfrac{M_{Tx} + (F_{Fz} + F_{Tz} - ma_z)y}{F_{Fy} + F_{Ty} + B - m(a_y + g)} \end{cases} \tag{1}$$

where $y = r(1-\cos q)$ and $x_{fe} = r(q-q_0) - r\sin q + r\sin q_0$, q_0 is the leg's rotation angle when begins a new walking cycle.

Note that a_x, a_y, and a_z are measured from an accelerometer, and q is sensed from the encoder. Furthermore, the fluid forces F_{Fx}, F_{Fy}, and F_{Fz} are related to robot velocity, i.e., v_x, v_y, v_z, which can be measured by DVL.

B. Desired ZMP

This subsection aims to derive the desired ZMP describing the required reaction forces of the prescribed locomotion. Unlike the motion states of the actual ZMP that arise from sensory measurements, the desired ZMPs are generated from a closed-loop CPG-based gait planner designed in [20].

We use support legs' desired rotation states to deduce the robot's desired velocity and acceleration. Then, using the Hopf oscillator that designs in Eq.(12) of [20], we deduce the desired rotation angle of ith leg as

$$q_{id} = \begin{cases} \dfrac{\theta_{si}}{2}\sin\left(\dfrac{\pi}{2}u_i\right) + \pi, & \text{if } \ v_i \le 0 \\ -\dfrac{\theta_{ti}}{2}\sin\left(\dfrac{\pi}{2}u_i\right) + 2\pi, & \text{if } \ v_i > 0 \end{cases} \tag{2}$$

where $\theta_{si} = k_\psi \Theta(i)(\psi - \psi_d) + \theta_{s0}$ and $\theta_{ti} = 2\pi - \theta_{si}$ are the support and swing angles of the ith leg. u_i and v_i are the state variables of the ith oscillator, the ith leg touches the terrain when $v_i \le 0$, k_ψ is a constant, $i \in (1, \cdots, 6)$ represents leg's serial number. θ_{s0} denotes the base value of the support angle, ψ and ψ_d are the yaw and desired yaw angles when the robot begins a new walking cycle. $\Theta(i)$ is a function to distinguish the robot's left and right legs. If i = 1, 3 or 5, $\Theta(i) = 1$. Otherwise, $\Theta(i) = -1$. The robot walks with tripod gaits. Thus, $u = u_1 = u_4 = u_5$ when legs 1, 4, and 5 are support legs. Otherwise, $u = u_2 = u_3 = u_6$. In addition, we can infer that $q_d = (0.5q_{1d} + 0.5q_{5d} + q_{4d})/2$ or $q_d = (0.5q_{2d} + 0.5q_{6d} + q_{3d})/2$. Finally, the desired angle of the virtual support legs is $q_d = \frac{\theta_{s0}}{2}\sin\left(\frac{\pi}{2}u\right) + \pi$, and $q_0 = \pi - \frac{\theta_{s0}}{2}$.

Taking the derivative of the q_d, we have

$$\begin{cases} \dot{q}_d = \dfrac{\pi\theta_{s0}}{4}\cos\left(\dfrac{\pi}{2}u\right)\dot{u} \\ \ddot{q}_d = \dfrac{\pi\theta_{s0}}{4}\left(\cos\left(\dfrac{\pi}{2}u\right)\ddot{u} - \dfrac{\pi}{2}\sin\left(\dfrac{\pi}{2}u\right)\dot{u}^2\right) \end{cases} \tag{3}$$

where $\ddot{u} = \delta\left(R^2 - u^2 - v^2\right)\dot{u} - 2\delta\left(u\dot{u} + v\dot{v}\right)u - 2\pi w\dot{v} + \zeta\sum_{j=1}^{6}(\cos\varphi_i^j\dot{u}_i - \sin\varphi_i^j\dot{v}_i)$, δ is the convergence factor, R is the limit ring radius, w is the oscillation frequency, and ζ is the coupling coefficient.

Based on the ZMP definitions in (1), we derive the desired forward and lateral ZMPs as

$$\begin{cases} X_{zmp}^d = x_{fe}^d + \dfrac{M_{Tz} - (F_{Fx}^d + F_{Tx} - ma_x^d)y_d}{F_{Fy}^d + F_{Ty} + B - m(a_y^d + g)} \\ Z_{zmp}^d = -\dfrac{M_{Tx} + (F_{Fz}^d + F_{Tz} - ma_z^d)y_d}{F_{Fy}^d + F_{Ty} + B - m(a_y^d + g)} \end{cases} \tag{4}$$

where x_{fe}^d and a_x^d are desired forward position and acceleration, y_d and a_y^d are vertical position and acceleration. F_{Fx}^d, F_{Fy}^d, and F_{Fz}^d are the desired forward, vertical, and lateral fluid forces related to the corresponding velocities and accelerations, i.e., v_x^d, v_y^d, v_z^d, a_x^d, a_y^d and a_z^d. These desired states are deduced as

$$\begin{cases} x_{fe}^d = r\left(q_d - q_0\right) - r\sin q_d + r\sin q_0 \\ y_d = r(1-\cos q_d), \quad v_x^d = r\dot{q}_d - r\dot{q}_d\cos q_d \\ v_y^d = r\dot{q}_d\sin q_d, \quad v_z^d = 0 \\ a_x^d = r(1-\cos q_d)\ddot{q}_d + r\sin q_d\dot{q}_d^2 \\ a_y^d = r\ddot{q}_d\sin q_d + r\dot{q}_d^2\cos q_d, \quad a_z^d = 0 \end{cases} \tag{5}$$

C. ZMP Bias

The previous subsections show that the actual and desired ZMPs can represent the actual and required reaction forces that the terrain acts on the robot. Thus, we indirectly extract unknown leg-terrain interaction force by removing the desired ZMP from the actual ZMP. The remainder of ZMP is called ZMP bias. Subtracting (4) from (1), we have

$$\begin{cases} X^e_{zmp} = \dfrac{M_{Tz} - (F_{Fx} + F_{Tx} - ma_x)y}{F_{Fy} + F_{Ty} + B - m(a_y + g)} \\ \qquad - \dfrac{M_{Tz} - (F^d_{Fx} + F_{Tx} - ma^d_x)y_d}{F^d_{Fy} + F_{Ty} + B - m(a^d_y + g)} \\ \qquad + r(q - q_d) - r(\sin q - \sin q_d) \\ Z^e_{zmp} = \dfrac{M_{Tx} + (F^d_{Fz} + F_{Tz} - ma^d_z)y_d}{F^d_{Fy} + F_{Ty} + B - m(a^d_y + g)} \\ \qquad - \dfrac{M_{Tx} + (F_{Fz} + F_{Tz} - ma_z)y}{F_{Fy} + F_{Ty} + B - m(a_y + g)} \end{cases} \tag{6}$$

Note that the presented ZMP bias has removed the effects caused by gravity, buoyancy, and thrust, leaving only inertial and fluid forces. It is consistent that different reaction forces result in different inertial and fluid forces by changing the support leg's rotation information. Thus, the ZMP bias can evaluate the leg-terrain interaction force.

Remark 1. *Apart from the reaction force, the support leg's inherent steady or transient control error is the other reason for the inertial and fluid forces change. That said, the leg's rotation angle fails to coincide with the desired value when using the controller to steer the leg without contact with the terrain. The inherent error is very little and generally less than 2°, which cannot cause a large change in inertial and fluid forces compared to the reaction force.*

Remark 2. *In fact, the legs' inertial and fluid forces are also parts of the robot's whole inertial and fluid forces. However, the forces are much smaller than those caused by the robot body and have been ignored via Assumption 1.*

IV. ZMP Bias Parameterization and Prediction

In practice, the measurement noises of proprioceptive sensors can make the actual ZMP and ZMP bias vary randomly, which may degrade the performance of compensating for leg-terrain interaction dynamics. Then, we need to smooth the ZMP bias. In addition, Assumption 3 shows that the terrain type will not change massively, and the closer two adjacent terrains can result in more similar deformable properties. Thus, we parameterize the previous ZMP bias as polynomials and use them to predict the current ZMP bias.

According to the definition of oscillator's frequency w, the time of a complete walking cycle of the robot is $T = \frac{1}{w}$. We collect the discrete time and kth complete walking cycle's forward and lateral ZMP biases as

$$\begin{cases} \mathcal{T}(k) = t_s[1, 2, \cdots, N_c]^\top \\ \mathcal{X}^e_{zmp}(k) = \left[X^e_{zmp}(kN_c + 1), \cdots, X^e_{zmp}(kN_c + N_c)\right]^\top \\ \mathcal{Z}^e_{zmp}(k) = \left[Z^e_{zmp}(kN_c + 1), \cdots, Z^e_{zmp}(kN_c + N_c)\right]^\top \end{cases} \tag{7}$$

where $N_c = T/t_s$ represents the number of total collections of one complete walking cycle, and t_s denotes the interval time for collecting.

We use a polynomial regression-based supervised learning method to fit the three discrete datasets in (7) as continuous forward and lateral ZMP biases related to several parameters and time. The supervised learning method contributes to smoothing the random measurement noises.

Specifically, the discrete forward and lateral ZMP biases of kth walking cycle are learned as $w_x^\top(k)\phi_x$ and $w_z^\top(k)\phi_z$, where $\phi_{(\cdot)} = \left[1, s, s^2, \cdots, s^{N-1}\right]^\top \in \mathbb{R}^N$ is the vector of ploynomial terms, $w_{(\cdot)} \in \mathbb{R}^N$ is a vector of parameters, $(\cdot)$ can be filled by x or z, N denotes the number of all polynomes, $s = \mathrm{mod}(t, T)$ is the remainder of t through dividing T, t is the elapsed time from the begining of walking.

Thus, $(k+1)$th walking cycle' ZMP biases are predicted by previous M walking cycles' parameterized polynomials as

$$\begin{cases} \hat{X}^e_{zmp}(k+1) = \displaystyle\sum_{j=k-M+1}^{k} \left(\lambda_j \cdot w_x^\top(j)\phi_x(j)\right) \\ \hat{Z}^e_{zmp}(k+1) = \displaystyle\sum_{j=k-M+1}^{k} \left(\lambda_j \cdot w_z^\top(j)\phi_z(j)\right) \end{cases} \tag{8}$$

where λ_j is a constant weight of jth walking cycle.

V. Controller Design

This section designs a controller for six hip joints and eight thrusters to follow the legs' desired rotation angles and compensate for the perceived interaction force.

A. Low-level control module

The low-level control module uses a PI controller to steer the legs and employs constant vertical thrusts to attach the robot to the terrain. To track the desired rotation angle, the simple but effective PI controller is designed as $\tau_i = K_{Pi}(q_i - q_{id}) + K_{Ii}\int(q_i - q_{id})dt$, where τ_i is the torque of ith leg, K_{Pi} and K_{Ii} are two constants, $i = 1, 2, \cdots, 6$. In addition, the basic vertical thrusts are designed as $T^b_1 = T^b_2 = T^b_3 = T^b_4 = T_0$, where $T_0 < 0$ is a constant. The lateral thrusts are set as zeros. That said, $T_5 = T_6 = T_7 = T_8 = 0$.

B. High-level control module

The high-level control module uses the calculated pitch and roll moments to compensate for leg-terrain interaction force, which is designed as

$$[T^a_1, T^a_2, T^a_3, T^a_4]^\top = \Gamma(C_T)[F_{Ry}\hat{Z}^e_{zmp}, -F_{Ry}\hat{X}^e_{zmp}]^\top \tag{9}$$

where T^a_k is the additional force of kth vertical thruster, $F_{Ry} = F_{Fy} + F_{Ty} + B - m(a_y + g)$, Γ is a function to calculate pseudo-inverse matrix, $C_T = \begin{bmatrix} \frac{l_1}{2} & -\frac{l_1}{2} & -\frac{l_1}{2} & \frac{l_1}{2} \\ \frac{l_2}{2} & \frac{l_2}{2} & -\frac{l_2}{2} & -\frac{l_2}{2} \end{bmatrix}$ denotes the force allocation matrix. Thus, the thrust of kth vertical thruster is $T_k = T^b_k + T^a_k$, where $k = 1, \cdots, 4$.

Remark 3. *Unlike end-to-end data-driven learning-based controllers, which learn the control policy through hundreds*

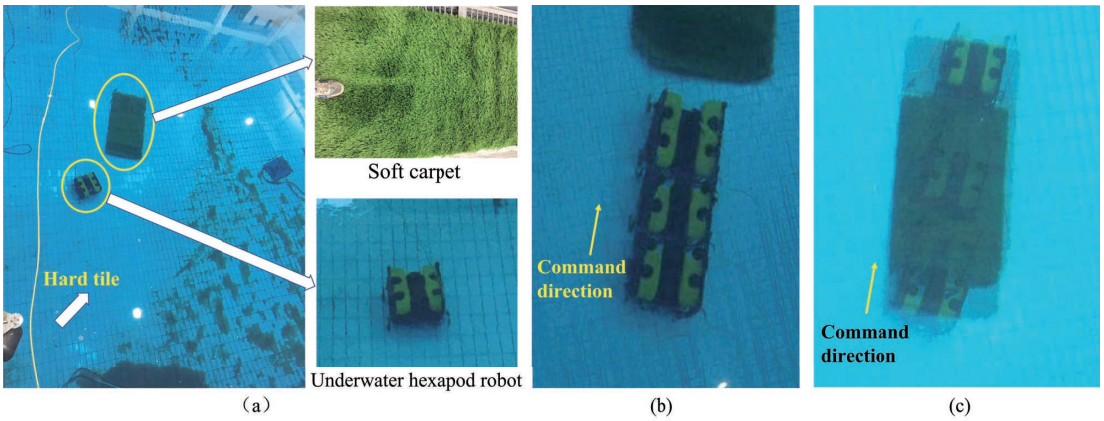

Fig. 6. Indoor pool experiment. (a) Experiment setup. (b) Snapshots of walking on the hard tile. (c) Snapshots of walking on the soft carpet.

or more training episodes, our two-layer controller is easy to implement because it uses the supervised learning method to parameterize online the ZMP biases and does not need the complex offline training. Furthermore, the low-level control module can provide foundational locomotion for the robot because of the constant vertical thrusts and PI controller. Finally, the high-level control module has clear physical meaning and explainability.

VI. EXPERIMENTS AND RESULTS

This section evaluates the proposed method for the robot and executes experiments in an indoor pool and a wild lake. Fig. 6 (a) shows the scenario of the indoor pool with the size of 20m×20m×8m, where the robot locates at the pool's bottom, and the soft carpet is placed on the hard tile. We conduct four groups of hardware experiments and provide their experimental objectives, results, and scenarios in Table II.

TABLE II
OVERVIEW OF FOUR GROUPS EXPERIMENTS.

Group	Verified performance	Result	Scenario
1	Terrain sensing	Figs. 7 (a) and (b) Table III	Pool
2	Parametrization and prediction	Fig. 7 (c) and (d) Table IV	Pool
3	Terrain-adaptive locomotion	Figs. 7 (e) and (f) Table V	Pool
4	Terrain-adaptive locomotion	Figs. 8 and 9 Table VI	Lake

A. Terrain Sensing

This subsection will verify whether the presented ZMP bias can perceive the leg-terrain interaction force. The experiments consist of two groups: walking on the soft carpet and the hard tile with constant and same yaw angles, and their snapshots are shown in Figs. 6 (b) and (c). Each group includes five tests with different vertical thruster forces, i.e., -30, -20, -15, -10, -5 N, which are called Test 1, 2, 3, 4, and 5. The total vertical forces applied to the robot body are -120, -80, -60, -40, and -20 N.

TABLE IV
AVERAGE ERRORS BETWEEN THE ESTIMATED AND PREDICTED ZMP BIAS

	$\lvert\hat{X}^e_{zmp} - X^e_{zmp}\rvert$ Mean [10^{-4} m]		$\lvert\hat{Z}^e_{zmp} - Z^e_{zmp}\rvert$ Mean [10^{-4} m]	
	Estimated	Predicted	Estimated	Predicted
Test 1	1.320	2.007	1.470	2.038
Test 2	1.444	3.195	1.689	3.432
Test 3	2.598	5.586	2.938	3.745
Test 4	1.879	4.228	0.752	0.0349
Test 5	1.212	3.3656	3.555	2.907
Test 6	2.422	6.750	2.011	2.161

Table III presents the average forward and lateral ZMP biases and the standard deviations of forward, vertical, and lateral accelerations. The deviations can describe the degree of the robot's vibration. The forward ZMP biases of walking on hard tile are about 50% larger than soft carpet. In addition, the acceleration's standard deviations of walking on hard tile are about 40% larger than on soft carpet. The comparison results match that the harder terrain results in a larger interaction force and demonstrate that the ZMP biases can indirectly perceive the leg-terrain interaction force.

The mean values of two lateral ZMP biases are about 10^{-3}m, around a tenth of forward ones. This is because the robot walks in the forward direction with a slight lateral acceleration, and the interaction forces can dramatically change the value of forward acceleration rather than lateral acceleration. Figs. 7 (a) and (b) show the forward and lateral ZMP biases while walking on the two terrains with -120 N vertical force.

B. Parametrization and Prediction

To verify the performance of parametrization and prediction, this subsection conducts six pool experiments, where the robot walks on the hard tile and each vertical thrust is -20 N. We use a 14th-order polynomial regression to parametrize the ZMP bias and the previous four walking cycles' estimated parameters to predict the current cycle's ZMP bias. Specifically, the coefficients in (8) are chosen as $M = 4$, $\lambda_{k-3} = 0.05$, $\lambda_{k-2} = 0.05$, $\lambda_{k-1} = 0.2$, and $\lambda_k = 0.7$.

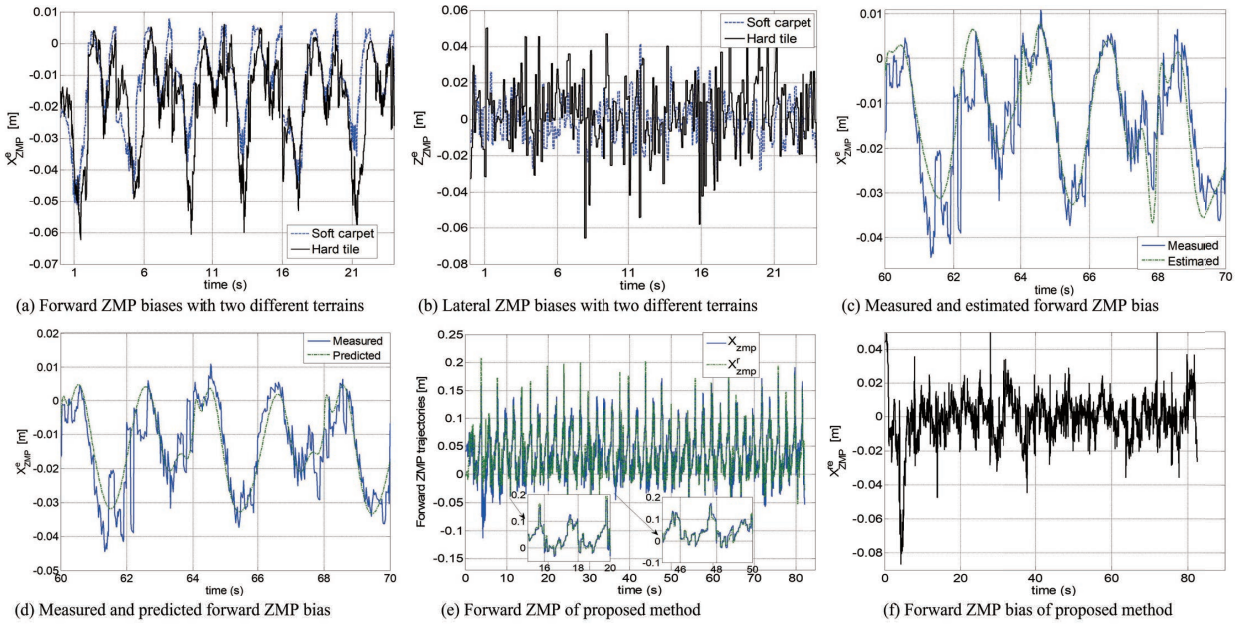

(a) Forward ZMP biases with two different terrains
(b) Lateral ZMP biases with two different terrains
(c) Measured and estimated forward ZMP bias
(d) Measured and predicted forward ZMP bias
(e) Forward ZMP of proposed method
(f) Forward ZMP bias of proposed method

Fig. 7. Experimental results of locomoting in indoor pool.

TABLE III
MEAN (μ) OF ZMP BIASES, STANDARD DEVIATION (σ) OF ACCELERATION OF THE ROBOT UNDER TWO TYPES OF EXPERIMENTS

	X^e_{zmp} μ [10^{-2} m]		Z^e_{zmp} μ [10^{-2} m]		a_x σ [m/s^2]		a_y σ [m/s^2]		a_z σ [m/s^2]	
	Tile	Carpet	Tile	Carpet	Tile	Carpet	Tile	Carpet	Tile	Carpet
Test 1	−1.826	−1.293	0.346	−0.070	0.342	0.232	0.310	0.145	0.319	0.1895
Test 2	−1.670	−1.380	−0.103	0.096	0.356	0.225	0.299	0.118	0.233	0.1722
Test 3	−1.909	−1.407	−0.018	0.357	0.303	0.212	0.291	0.099	0.216	0.1554
Test 4	−2.102	−1.615	0.082	0.101	0.244	0.201	0.2197	0.138	0.219	0.1744
Test 5	−3.0932	−1.312	−0.3739	−0.2584	0.237	0.123	0.196	0.117	0.313	0.1459

TABLE V
AVERAGE VALUES OF X^{re}_{zmp} AND Z^{re}_{zmp} OF EACH INDOOR POOL TESTS

	Test 1	Test 2	Test 3	Test 4	Test 5	Test 6	Test 7	Test 8	Test 9	Mean value
X^{re}_{zmp} [10^{-4}m]	−1.1474	1.3814	5.9702	−2.9005	7.6053	2.8255	2.8622	3.5536	−1.0393	**2.1234**
Z^{re}_{zmp} [10^{-3}m]	−0.1642	1.3655	1.1507	−2.6632	−1.5860	2.3381	−2.2976	−0.4406	−0.1739	**-0.2746**

Figs. 7 (c) and (d) show the estimated and predicted ZMP biases. Table IV provides the average errors between the measured and estimated/predicted ZMP biases. We note that the predicted average error's magnitude is almost twice that of the estimated one. There are two factors accounting for this phenomenon. The predicted error is based on several collected estimated ZMP biases. In addition, proprioceptive sensor noises are stochastic and different in diverse walking cycles. Polynomials can approximate the bias according to the corresponding noises but fail to match the noises of the current walking cycle. This is the other reason to enlarge the predicted error. Even so, predicting accuracy meets practical requirements because the forward ZMP bias's predicted errors are about 1% of the forward ZMP bias in Table III.

C. Terrain-adaptive Locomotion in Pool

To study whether our method can reduce the adverse effects caused by leg-terrain interaction dynamics, we conduct nine pool experiments where the robot walks in a constant direction on hard tile, and each basic vertical thrust is set as -20 N.

The ZMP biases in (6) directly reflect the leg-terrain interaction force. To observe whether the dynamics is compensated, we define the other set of ZMP biases as $X^{re}_{zmp} = X_{zmp} - X^r_{zmp}$ and $Z^{re}_{zmp} = Z_{zmp} - Z^r_{zmp}$, where X^r_{zmp} and Z^r_{zmp} are reference forward and lateral ZMPs determined by basic thruster forces and the prescribed walking motion, whereas the X^d_{zmp} and Z^d_{zmp} in (4) are determined by the actual thruster forces and the prescribed walking motion.

Table V provides the average values of X^{re}_{zmp} and Z^{re}_{zmp} of

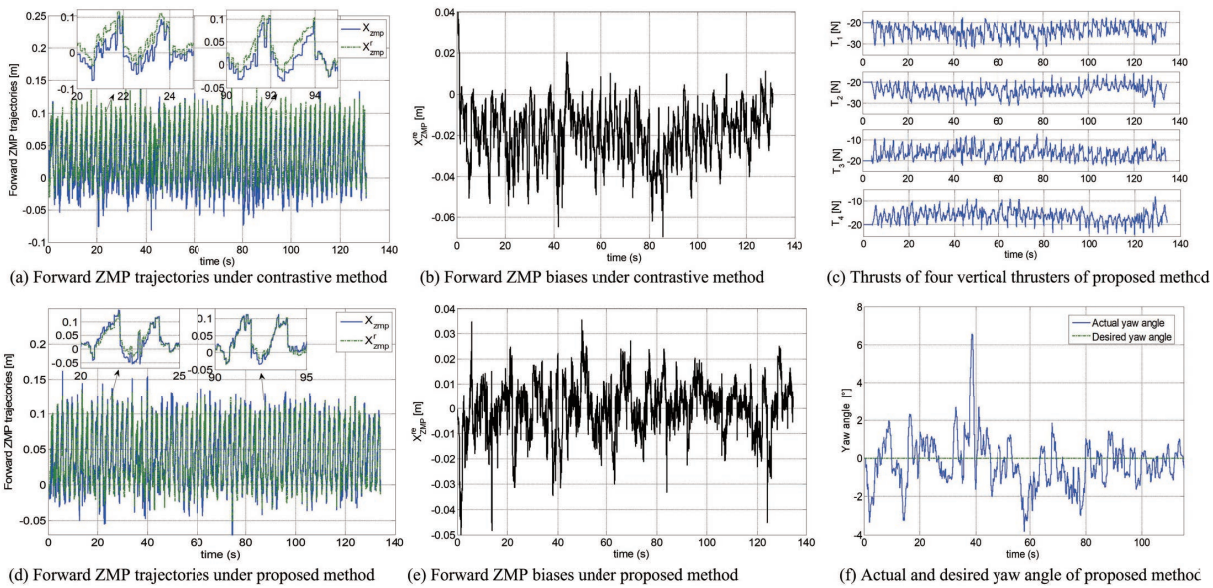

Fig. 8. Experimental results of locomoting in uncertain wild environment.

each Test. Fig. 7 (e) presents the trajectories of actual ZMP X_{zmp} and reference forward ZMP X^r_{zmp} of Test 1. Fig. 7 (f) shows forward ZMP biases X^{re}_{zmp} of Test 1. The mean value of nine forward ZMP biases in Table V is 2.1234×10^{-4} m, which is much smaller than 1.67×10^{-2} m of Test 2 in Table III. Then it demonstrates that the proposed control method can compensate for the adverse effects caused by leg-terrain interaction force and achieve the goal of smooth traversing.

D. Terrain-adaptive Locomotion in Lake

This subsection aims to verify the superior performance of the proposed method through several contrastive lake experiments, where the contrastive method only uses the base control module to steer the robot. The lake's terrain has uncertain deformable properties, which may result in uncertain interaction forces.

We conduct four groups of tests, each containing two experiments that use the proposed and contrastive methods to steer the robot. The basic vertical thrust T_0 and the lateral thrust of each test are set as -20 N and 0 N, respectively.

Fig. 8 provides the experimental results of locomoting in the wild lake with unknown terrain, including the comparisons of X_{zmp} and X^{re}_{zmp} between the proposed method and contrastive method, and vertical thrusts and yaw angle. Figs. 8 (a) and (d) show that the proposed method can track the reference forward ZMP trajectory precisely. The results in Figs. 8 (b) and (e) also verify this conclusion. The robot's yaw angle in Fig. 8 (f) can converge to the desired value. We present the quantitative results of the proposed and contrastive methods in Table VI. The presented method achieves the forward ZMP bias with a magnitude of about 1.5 $\times10^{-4}$ m, much smaller than the approximate magnitude of 1.5 $\times10^{-2}$ m in the contrastive method. Fig. 9 presents the perceived leg-terrain interaction forces of the robot that walks in the wild lake. Fig. 9 (a) provides two sets of perceived pitch moments, showing that the constrastive moment is much larger than the proposed one. Then, the proposed controller can reduce the pitch moment for stable walking. Fig. 9 (b) presents two groups of perceived vertical forces. They are close to each other because the vertical thruster forces of the two experiments are the same. As a result, we have obtained the following findings.

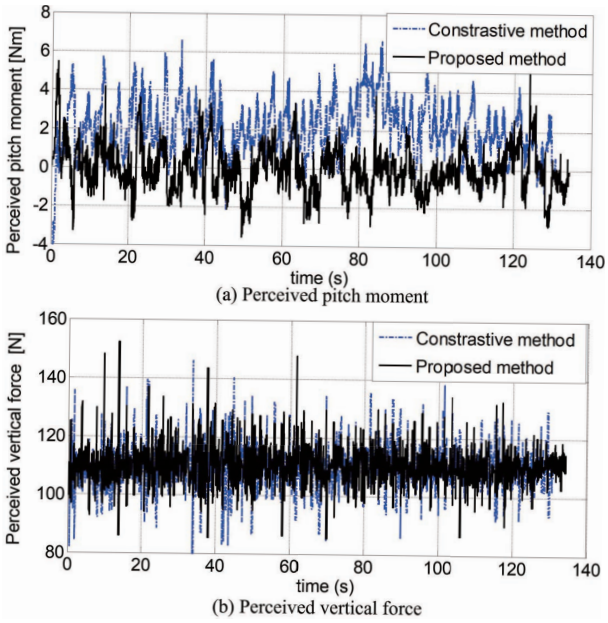

Fig. 9. Perceived Leg-terrain interaction forces.

1) Fig. 8 (b) shows that the average values of X^{re}_{ZMP} are smaller and smaller because the terrain becomes softer and softer while closer to the lake's center. The phenomenon is consistent with the lake's actual topographic feature and demonstrates the proposed method's effectiveness in perceiving the interaction force.
2) Figs. 8 (a), (d) and Fig. 9 (a) reveal that the proposed

IEEE Robotics & Automation Magazine (RAM) paper, presented at ICRA 2024, Yokohama, Japan. Cite as RAM paper.

TABLE VI
MEAN OF X^{re}_{zmp} AND Z^{re}_{zmp} OF EACH WILD LAKE TESTS

	X^{re}_{zmp} μ [10^{-4} m]		Z^{re}_{zmp} μ [10^{-4} m]	
	Contrastive	Proposed	Contrastive	Proposed
Group 1	-194.1	1.35	4.136	-4.798
Group 2	-154.39	2.676	-4.359	-7.492
Group 3	-150.3433	0.971	4.043	5.061
Group 4	-164.56	3.445	-3.363	-7.933

method can steer the robot tracking the reference forward ZMP and traversing unknown terrains via regulating vertical thrusters to provide needed roll and pitch moments.

E. Discussion

The presented terrain-adaptive locomotion controller can be expanded to other general scenarios or robots.

1) The method of generating prescribed motion is not limited to the CPG-based gait planner. The ZMP biases in (6) rely on the states of the robot's desired position, velocity, and acceleration. Besides the CPG-based gait planner, many other methods, such as RRT-based and optimal-based planners, can also provide these desired values.
2) The ZMP bias based perceiving method can also be applied to other legged robots through slight modifications, e.g., re-deriving the desired position, velocity, and acceleration according to the leg's shape.
3) The proposed method can also steer the robot climbing other underwater structures with large dip angles, such as ship hull and drilling platform. The component forces caused by gravity and buoyancy on the body-fixed frame may change because the robot's attitude differs. Thus, we should project these forces into the body-fixed frame and re-derive the ZMPs.

VII. CONCLUSIONS

This paper has presented a terrain-adaptive locomotion control method for an underwater hexapod robot to traverse diverse terrains with unknown deformable properties smoothly. By performing extensive hardware experiments on an indoor pool and lake, we have demonstrated that the proposed ZMP bias can be used to perceive the leg-terrain interaction force and the presented two-layer controller can compensate for it by regulating thruster forces. In addition, our method has the following two promising prospects in practical applications.

1) The proposed ZMP bias only relies on some common proprioceptive sensors, which has clear physical meanings and the advantage of easy implementation.
2) The two-layer controller, which uses a base control module to achieve basic locomotion and employs a high-level control module to regulate thruster forces, can be used to track the prescribed locomotion motion smoothly. Each layer has its own control goal, and the two-layer controller can be easily extended to other robots simultaneously driven by legs and thrusters.

REFERENCES

[1] N. M. Graf, A. M. Behr, and K. A. Daltorio, "Dactyls and inward gripping stance for amphibious crab-like robots on sand," *Bioinspiration & Biomimetics*, vol. 16, no. 2, p. 026021, 2021.

[2] Y. Chen, G. Clifton, N. M. Graf, K. Durand, J. Taylor, Y. Gong, J. E. Grezmak, and K. A. Daltorio, "Optimal planar leg geometry in robots and crabs for idealized rocky terrain," *Bioinspiration & Biomimetics*, vol. 17, no. 6, p. 066009, 2022.

[3] X. Xiong, A. D. Ames, and D. I. Goldman, "A stability region criterion for flat-footed bipedal walking on deformable granular terrain," in *Proceedings IEEE/RSJ International Conference on Intelligent Robots and Systems*. IEEE, 2017, pp. 4552–4559.

[4] W. Bosworth, J. Whitney, S. Kim, and N. Hogan, "Robot locomotion on hard and soft ground: Measuring stability and ground properties in-situ," in *Proceedings IEEE International Conference on Robotics and Automation*. IEEE, 2016, pp. 3582–3589.

[5] S. Fahmi, M. Focchi, A. Radulescu, G. Fink, V. Barasuol, and C. Semini, "Stance: Locomotion adaptation over soft terrain," *IEEE Transactions on Robotics*, vol. 36, no. 2, pp. 443–457, 2020.

[6] G. Romualdi, S. Dafarra, and D. Pucci, "Modeling of visco-elastic environments for humanoid robot motion control," *IEEE Robotics and Automation Letters*, vol. 6, no. 3, pp. 4289–4296, 2021.

[7] A. Nikolakakis, I. Kontolatis, N. Cherouvim, P. Chatzakos, and E. Papadopoulos, "Implementation of a quadruped robot pronking/bounding gait using a multipart controller," in *Proceedings Dynamic Systems and Control Conference*, 2010.

[8] V. Vasilopoulos, I. S. Paraskevas, and E. G. Papadopoulos, "Compliant terrain legged locomotion using a viscoplastic approach," in *Proceedings IEEE/RSJ International Conference on Intelligent Robots and Systems*. IEEE, 2014, pp. 4849–4854.

[9] V. Vasilopoulos, K. Machairas, and E. Papadopoulos, "Quadruped pronking on compliant terrains using a reaction wheel," in *Proceedings IEEE International Conference on Robotics and Automation (ICRA)*. IEEE, 2016, pp. 3590–3595.

[10] V. Vasilopoulos, I. S. Paraskevas, and E. G. Papadopoulos, "Monopod hopping on compliant terrains," *Robotics and Autonomous Systems*, vol. 102, pp. 13–26, 2018.

[11] K. Ho, T. Peynot, and S. Sukkarieh, "A near-to-far non-parametric learning approach for estimating traversability in deformable terrain," in *2013 IEEE/RSJ International Conference on Intelligent Robots and Systems*. IEEE, 2013, pp. 2827–2833.

[12] A. H. Chang, C. M. Hubicki, J. J. Aguilar, D. I. Goldman, A. D. Ames, and P. A. Vela, "Learning terrain dynamics: A gaussian process modeling and optimal control adaptation framework applied to robotic jumping," *IEEE Transactions on Control Systems Technology*, vol. 29, no. 4, pp. 1581–1596, 2020.

[13] J. Lee, J. Hwangbo, L. Wellhausen, V. Koltun, and M. Hutter, "Learning quadrupedal locomotion over challenging terrain," *Science robotics*, vol. 5, no. 47, p. eabc5986, 2020.

[14] K. Ho, T. Peynot, and S. Sukkarieh, "Nonparametric traversability estimation in partially occluded and deformable terrain," *Journal of Field Robotics*, vol. 33, no. 8, pp. 1131–1158, 2016.

[15] X. A. Wu, T. M. Huh, R. Mukherjee, and M. Cutkosky, "Integrated ground reaction force sensing and terrain classification for small legged robots," *IEEE Robotics and Automation Letters*, vol. 1, no. 2, pp. 1125–1132, 2016.

[16] X. A. Wu, T. M. Huh, A. Sabin, S. A. Suresh, and M. R. Cutkosky, "Tactile sensing and terrain-based gait control for small legged robots," *IEEE Transactions on Robotics*, vol. 36, no. 1, pp. 15–27, 2019.

[17] J. Bednarek, M. Bednarek, L. Wellhausen, M. Hutter, and K. Walas, "What am I touching? learning to classify terrain via haptic sensing," in *Proceedings International Conference on Robotics and Automation*. IEEE, 2019, pp. 7187–7193.

[18] J. Zürn, W. Burgard, and A. Valada, "Self-supervised visual terrain classification from unsupervised acoustic feature learning," *IEEE Transactions on Robotics*, vol. 37, no. 2, pp. 466–481, 2021.

[19] M. Vukobratović and B. Borovac, "Zero-moment point–thirty five years of its life," *International journal of humanoid robotics*, vol. 1, no. 1, pp. 157–173, 2004.

[20] F. Ma, W. Yan, L. Chen, and R. Cui, "CPG-based motion planning of hybrid underwater hexapod robot for wall climbing and transition," *IEEE Robotics and Automation Letters*, vol. 7, no. 4, pp. 12 299 – 12 306, 2022.

IEEE Robotics & Automation Magazine (RAM) paper, presented at ICRA 2024, Yokohama, Japan. Cite as RAM paper.